⌘ *Author's Choice*

THE JOURNAL OF BIOLOGICAL CHEMISTRY VOL. 287, NO. 10, pp. 7182–7189, March 2, 2012

Structural Analysis of the *Plasmodium falciparum* Erythrocyte Membrane Protein 1 (*Pf*EMP1) Intracellular Domain Reveals a Conserved Interaction Epitope*[S]

Received for publication, December 5, 2011, and in revised form, January 10, 2012 Published, JBC Papers in Press, January 16, 2012, DOI 10.1074/jbc.M111.330779

Christina Mayer[‡1], **Leanne Slater**[‡1], **Michele C. Erat**[‡], **Robert Konrat**[§], **and Ioannis Vakonakis**[‡1,2]

From the [‡]*Department of Biochemistry, University of Oxford, Oxford OX1 3QU, United Kingdom and the* [§]*Department of Biomolecular Structural Chemistry, University of Vienna, 1030 Vienna, Austria*

Background: *Pf*EMP1 localization and connection to the red blood cell cytoskeleton is necessary for cytoadherence.
Results: The *Pf*EMP1 intracellular domain (ATS) is structurally conserved and interacts directly with a novel parasite protein through a flexible epitope.
Conclusion: The ATS epitope mediate interactions that may be critical for cytoadherence.
Significance: This is the first demonstration of ATS interacting with PHIST domains.

***Plasmodium falciparum*-infected red blood cells adhere to endothelial cells, thereby obstructing the microvasculature. Erythrocyte adherence is directly associated with severe malaria and increased disease lethality, and it is mediated by the *Pf*EMP1 family. *Pf*EMP1 clustering in knob-like protrusions on the erythrocyte membrane is critical for cytoadherence, however the molecular mechanisms behind this system remain elusive. Here, we show that the intracellular domains of the *Pf*EMP1 family (ATS) share a unique molecular architecture, which comprises a minimal folded core and extensive flexible elements. A conserved flexible segment at the ATS center is minimally restrained by the folded core. Yeast-two-hybrid data and a novel sequence analysis method suggest that this central segment contains a conserved protein interaction epitope. Interestingly, ATS in solution fails to bind the parasite knob-associated histidine-rich protein (KAHRP), an essential cytoadherence component. Instead, we demonstrate that ATS associates with PFI1780w, a member of the *Plasmodium* helical interspersed sub-telomeric (PHIST) family. PHIST domains are widespread in exported parasite proteins, however this is the first specific molecular function assigned to any variant of this family. We propose that PHIST domains facilitate protein interactions, and that the conserved ATS epitope may be targeted to disrupt the parasite cytoadherence system.**

Erythrocytes are extensively remodeled by *Plasmodium falciparum* through the creation of multiple membrane compartments, modifications of the host cytoskeleton and the development of dense protrusions (knobs) on the erythrocyte surface (1, 2). Proteins from the parasite *Plasmodium falciparum* erythrocyte membrane protein 1 (*Pf*EMP1)[3] family (3) localize on knobs (4) and bind endothelial cell surface molecules through their variable extracellular domains. *Pf*EMP1 diversity leads to a variable antigenic envelope on the erythrocyte surface allowing evasion of the host immune response (5); at the same time, *Pf*EMP1-mediated adhesion promotes formation of infected erythrocyte clumps (6) and their sequestration in the microvasculature (7). Excessive erythrocyte sequestration is directly linked to tissue damage, organ failure, and increased disease lethality in *P. falciparum* infections.

Importantly, effective cytoadherence requires *Pf*EMP1 localization on knobs as well as the creation of mechanical links to the host cytoskeleton that can resist the hydrodynamic forces exerted by blood flow (8). The intracellular domain of *Pf*EMP1, ATS, is well conserved in the *Pf*EMP1 family (3) and likely constitutes the focal point of an intracellular protein network that enables localization and creates mechanical connections. A number of past studies have focused on the putative interaction between ATS and KAHRP (8), an intracellular parasite component essential for cytoadherence. Similar to *Pf*EMP1, KAHRP localizes in knobs, thereby placing these two proteins in close proximity *in vivo*. Recombinant KAHRP and ATS fragments have been shown to bind when immobilized on surfaces (9–11), on the basis of which the ATS-KAHRP interaction is widely accepted in the malaria field. However, to date there have been no biophysical studies of ATS or its interactions.

Here, we present an analysis of the ATS structure that reveals a conserved protein interaction epitope in this domain. Using

* This work was supported by the Wellcome Trust (to C. M. and I. V.) and the Marie Curie Fellowships programme (FP7) and the Royal Society (to M. C. E.).

The atomic coordinates and structure factors (code 2LKL) have been deposited in the Protein Data Bank, Research Collaboratory for Structural Bioinformatics, Rutgers University, New Brunswick, NJ (http://www.rcsb.org/).

Chemical shift assignments have been deposited in the BioMagResBank under accession numbers 16911 (ATS-Core) and 17999 (ATS-FL).

⌘ *Author's Choice*—Final version full access.

[S] This article contains supplemental Figs. S1–S12 and Table S1.

[1] These authors contributed equally to this work.

[2] To whom correspondence should be addressed: Department of Biochemistry, University of Oxford, South Parks Road, Oxford OX1 3QU, UK. Tel.: 44-0-865-613362; Fax: 44-0-1865-613201; E-mail: ioannis.vakonakis@bioch.ox.ac.uk.

[3] The abbreviations used are: *Pf*EMP1, *Plasmodium falciparum* erythrocyte membrane protein 1; ATS, acidic terminal segment; KAHRP, knob-associated histidine-rich protein; PHIST, *Plasmodium* helical interspersed subtelomeric; AUC, analytical ultracentrifugation; SLS, static light scattering; SAXS, small-angle x-ray scattering; HSQC, heteronuclear single quantum coherence; EOM, ensemble optimization method.

solution NMR spectroscopy and small angle x-ray scattering (SAXS) we show that ATS domains across the *Pf*EMP1 family share a molecular architecture dominated by flexible segments. ATS contains a single folded core composed of two distinct helical elements that are located far apart in the sequence. In contrast to previous ATS-KAHRP reports, we observed no detectable binding between these two proteins in solution. Our analysis of existing yeast-two-hybrid (Y2H) data, coupled to a novel computational prediction method presented here, suggested the presence of a conserved interaction epitope on a flexible ATS segment; the Y2H data also provided a series of putative ATS targets beyond KAHRP. Solution experiments supported this analysis by demonstrating an ATS interaction for a novel parasite protein, PFI1780w, comprising a PHIST-type domain (12); this is the first function assigned to this parasite-specific protein class. We suggest that the conserved ATS epitope and its interactions may present an attractive target for disrupting the *P. falciparum* cytoadherence system.

EXPERIMENTAL PROCEDURES

Protein Production and Purification—Details of protein preparation are presented in supporting methods. Briefly, ATS and its subfragments were prepared by meta-affinity chromatography under denaturing conditions followed by refolding, ion exchange and size exclusion chromatography. Native ATS production was performed in a similar fashion in the absence of urea. KAHRP fragments and PFI1780w were prepared by glutathione-Sepharose affinity and size exclusion chromatography. For fluorescent labeling of ATS-FL an engineered variant carrying the Q150C amino acid substitution was incubated with fluorescein-5-maleimide; unreacted label was removed by size exclusion chromatography.

Biophysical Characterization—Protein identity was confirmed by MALDI-TOF mass spectrometry. Analytical ultracentrifugation (AUC) experiments were performed on 30 μM protein samples in PBS (150 mM NaCl, 20 mM Na_2HPO_4 pH 7.4) supplemented with 1 mM Tris(2-carboxyethyl)phosphine using a Beckman Optima XL-I analytical ultracentrifuge. The AUC run was conducted at 4 °C and 15,000 rpm, using absorbance at 280 nm for monitoring the equilibrium. Circular dichroism (CD) spectra were collected in PBS supplemented with 1 mM DTT and at a protein concentration of 25 μM. A Chirascan spectropolarimeter with a 0.1 cm path length (AppliedPhotophysics) was used for CD. Thermal stability experiments were performed using a 1 °C/min temperature ramp between 10 °C and 90 °C and monitored by CD at 222 nm. Static light scattering (SLS) experiments were performed on samples of 2–4 mg/ml concentration in PBS, using an S-200 analytical size exclusion chromatography column (GE LifeSciences) connected in-line to miniDAWN TREOS light scattering and Optilab T-rEX refractive index detectors (Wyatt Technology). Fluorescence anisotropy experiments were performed using a PHERAstar FS microplate reader (BMG Labtech). Fluorescein-labeled ATS-FL at 0.5 μM concentration in NMR buffer was excited at 485 nm and polarization was recoded at 520 nm.

NMR Spectroscopy and Structure Determination—All NMR experiments were performed at 25 °C or 10 °C in NMR buffer (50 mM NaCl, 20 mM Na_2HPO_4 pH 7.0, 2 mM DTT) supplemented with 5% v/v D_2O, 0.02% w/v NaN_3 and 50 μM DSS. To overcome the lack of chemical shift dispersion in unstructured segments of proteins we performed chemical shift assignments by correlating multiple three-dimensional experiments (CBCA(CO)NH, CBCANH, HBHA(CO)NH, HBHANH, HNCO, HCACO, HCA(CO)N). This allowed us to follow the protein backbone connectivity by relying on both carbon and proton resonances. NMR dynamics experiments, acquisition and evaluation of structure restraints and setup of structure calculations were performed in a manner analogous to that described previously (13). For NMR titrations of ^{15}N-enriched and nonenriched components, care was taken that the pH of samples did not deviate more than 0.02 units.

Small Angle X-ray Scattering (SAXS) Data Collection and Processing—SAXS data were collected at the BioSAXS beamline at ESRF (ID14–3) at 20 °C and 0.931 Å wavelength. Samples in PBS buffer were centrifuged at 189,000 × *g* for 1 h just prior to data collection, and supplemented with 5 mM DTT. Sample buffer and proteins in four different concentrations (15 mg/ml, 10 mg/ml, 5 mg/ml, and 2.5 mg/ml) were measured while flowing through a thin capillary (20 μl of flow per measurement, 100 s flow time). On-site inspection of data showed no indication of radiation damage. A sample of bovine serum albumin was measured as control. Buffer subtraction, intensity normalization, and data merging for the different sample concentrations was performed using PRIMUS (14). Selection of best molecular models that fit the SAXS data were performed using the ensemble optimization method (EOM) (15).

Meta-structure Analysis—The meta-structure secondary structure analysis has been presented elsewhere (16). Use of this tool for identification of protein interaction epitopes is detailed in supporting methods. Briefly, the quantitative per-residue topology information derived by meta-structure analysis of ATS-FL (supplemental Fig. S2) was compared with similar information derived from the protein interaction interfaces of 1750 complexes in the RCSB. The degree of similarity over a sliding residue window is expressed as the PII score. PII beyond 1000 are considered to be highly significant.

Sequences and Notes—We define the *Pf*EMP1 ATS as the protein C-terminal fragment following the predicted transmembrane helix, typically beginning with three lysine residues. Thus, for variant PF08_0141 the ATS comprises residues 2466–2858 of that entry; similar criteria were used to define the ATS of other *Pf*EMP1 genes. Amino acid residue numbering starts at the first residue following the transmembrane segment. DNA encoding for the PF08_0141 and PFF0845c ATS were obtained by Drs. Amit Sharma (ICGEB, India) and Matthew Higgins (University of Oxford, UK), respectively. Other ATS in this study and the PFI1780w gene were amplified from a *P. falciparum* cDNA library (MRA-898) from the Malaria Research and Reference Reagent Resource Center (MR4, ATCC). The KAHRP clone was obtained from the same source (MRA-6).

Chemical shift assignments have been deposited in the BioMagResBank under accession numbers 16911 (ATS-Core) and 17999 (ATS-FL). The structure and structure calculation restraints for ATS-Core have been deposited in the RCSB under accession number 2LKL.

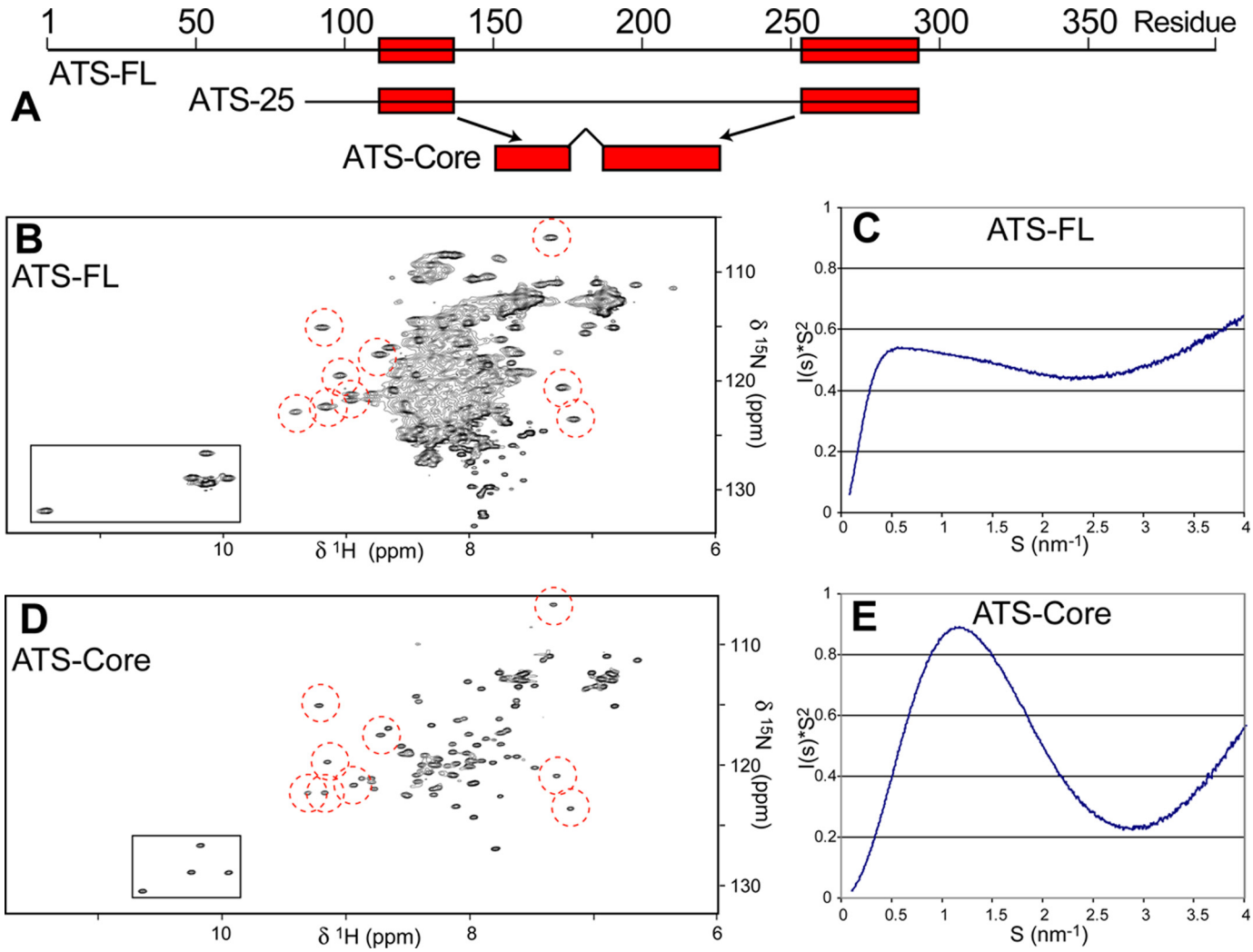

FIGURE 1. **Molecular architecture of the ATS domain of *Pf*EMP1.** *A*, schematic representation of the ATS-FL, ATS-25, and ATS-Core constructs. Residue numbering starts at the end of the preceding transmembrane segment. Red segments correspond to the two well-structured α-helical parts of ATS-FL that, together, comprise ATS-Core. *B*, NMR ^{1}H-^{15}N HSQC spectra of ATS-FL at 25 °C. Distinct resonances, corresponding to the structured part of this construct, are circled in *red*. Trp sidechain resonances are *boxed*. *C*, Kratky representation of SAXS data from ATS-FL at 20 °C. *D* and *E*, similar NMR and SAXS spectra from ATS-Core. Note the persistence of dispersed resonances (*red circles*) across ATS constructs.

RESULTS

ATS Is Dominated by Flexible Segments—We initiated our structural studies using the full-length ATS domain from *Pf*EMP1 variant PF08_0141, henceforth referred to as ATS-FL (Fig. 1*A*). This particular ATS variant has been previously made in *Escherichia coli* (17), thereby facilitating recombinant protein production for biophysical analysis. Our initial attempts revealed ATS-FL to be sensitive to proteolysis when made under native conditions, which limited the amounts of protein that were obtained. Yields improved when producing this protein in *E. coli* inclusion bodies, followed by denatured extraction and a simple refolding protocol. Solution NMR ^{1}H-^{15}N heteronuclear single quantum coherence (HSQC) spectra, which provide per-residue structural information, showed no significant difference between ATS-FL produced under native or denatured conditions (supplemental Fig. S1). Thus, we judged our refolding protocol to be successful in reproducing the native protein state.

The NMR spectra of ATS-FL were dominated by many sharp and heavily overlapping resonances at the center of the data (Fig. 1*B*). Such resonances are typically associated with unstructured parts of proteins, such as flexible loops or linkers between domains. In contrast, we observed relatively few distinct resonances away from the center, which would correspond to folded elements in the protein. Given the length of ATS-FL (393 residues) and the small number of dispersed resonances seen, we concluded that this protein is primarily unstructured. This conclusion was further supported by computational and experimental means. The predicted average residue compactness (16, 18) of ATS-FL is ~215, which lies between the threshold for completely unfolded chains and the average value of globular proteins (supplemental Fig. S2). The Kratky representation of SAXS data from ATS-FL has a largely flat appearance as opposed to the characteristic bell-shaped curve of structured proteins (Fig. 1*C*, raw data shown in supplemental Fig. S3). We estimated the radius of gyration (R_g) for ATS-FL from the same data using the Guinier approximation as being ~4.97 nm, a value much larger than expected (2.15 nm) for globular proteins of this size (19). CD spectra of ATS-FL display a minimum at 205 nm, indicative of random coil, as well

as α-helical propensity at 222 nm (supplemental Fig. S4). The α-helical signal decreases cooperatively upon thermal unfolding, which supports the existence of a small structured element in ATS-FL. Finally, ATS-FL does not form dimers in solution as suggested earlier by size-exclusion chromatography (17). Instead, the molecular size estimated by SAXS (supplemental Fig. S3), AUC (supplemental Fig. S5) and SLS (supplemental Fig. S5) closely corresponds to that of the monomer under physiological conditions. It is likely that an increased hydrodynamic radius, caused by the flexible nature of ATS, was responsible for the earlier dimer report.

We attempted to isolate the structured part of ATS-FL through serial truncations, however our results were initially unsuccessful. Sequence analysis using a number of disorder prediction algorithms also failed to indicate the structured protein parts (supplemental Fig. S2). In contrast, the meta-structure secondary structure analysis of ATS (16) allowed us to clearly distinguish between extended segments which are likely to be flexible, and α-helical segments (supplemental Fig. S2). Results from this analysis agreed well with NMR chemical shift deviations from random coil (supplemental Fig. S6) obtained from an ATS fragment spanning residues 87–292 (ATS-25, Fig. 1*A* and supplemental Fig. S7). Both methods revealed two α-helical regions spanning residues 112–136 and 254–292, and separated by a large flexible segment. No other structured segment was suggested by meta-structure or by NMR assignments of the remaining ATS (supplemental Fig. S6).

Based on this information, we designed a construct composed only of residues 109–136 and 245–292 (*ATS-Core*, Fig. 1*A*), thereby lacking all flexible elements. The NMR spectra of ATS-Core show substantial chemical shift dispersion (Fig. 1*D*) and the Kratky plot features a well-defined parabola (Fig. 1*E*), evidence which supports the fully folded state of this construct. The CD spectra of ATS-Core confirm that it is fully helical and cooperatively folded (supplemental Fig. S4). Thus, we conclude that the molecular architecture of ATS-FL is dominated by three large flexible segments at the protein N terminus, C terminus, and center, as well as a small α-helical folded core.

The ATS Architecture Is Conserved—P. falciparum isolate 3D7 comprises 59 *Pf*EMP1 variants, whose ATS domains range from 348 to 493 residues in length and share ~40% to 85% pair wise sequence identity (20). To test the degree of structural similarity between ATS-FL and other variants, we produced ATS domains from *Pf*EMP1 genes PF08_0131, PFB1055c, PFC1120c, PFF0010w, and PFF0845c. These genes cover all four sequence clusters of ATS (20), and show significant sequence divergence especially at the protein C terminus (supplemental Fig. S8). However, the NMR spectra of all variants were highly similar to that of ATS-FL, showing large resonance overlap indicative of extensive disorder and only minor folded parts (supplemental Fig. S9). Further, SAXS data from variant PFF0845c display a characteristically flat Kratky plot similar to ATS-FL (supplemental Fig. S10), and provide a R_g estimate (4.23 nm) much larger than expected for globular proteins (2.05 nm). Because ATS PFF0845c was purified under native conditions, these results support our earlier observations using refolded ATS-FL.

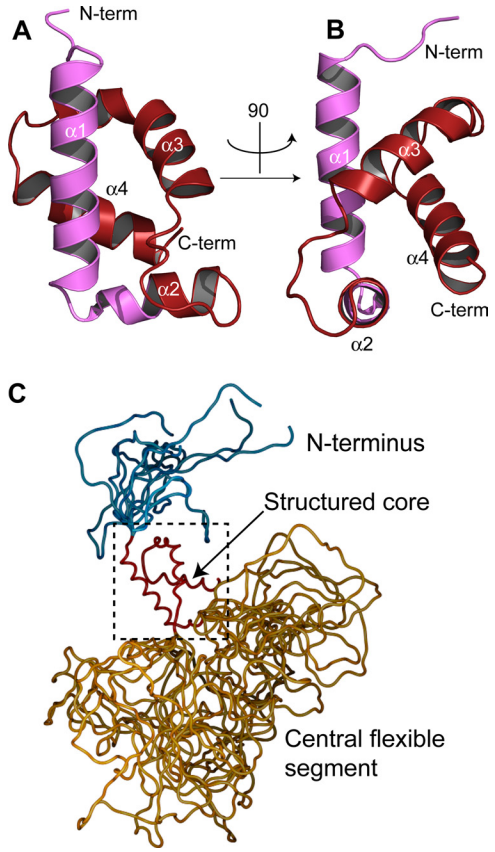

FIGURE 2. **Structure of ATS-Core and ATS-25.** *A* and *B*, schematic representation of the ATS-Core structure in two orthogonal orientations. The helical elements and protein termini are denoted. Shown in *magenta* and *red* are the segments arising from the first and second distinct α-helical regions of ATS, respectively. *C*, representative members from the ATS-25 structure ensemble calculated from NMR restraints and based on ATS-Core. The structured core is shown in *red*, the central flexible segment in *gold*, and the construct N terminus in *blue*. The flexible segments of this construct do not adopt a unique structure but, rather, explore a wide range of conformations and a large volume of space, as illustrated in this ensemble.

Constructs corresponding to ATS-Core from all variants show substantial NMR chemical shift dispersion (supplemental Fig. S9) and yield α-helical CD spectra that melt cooperatively under thermal unfolding (supplemental Fig. S4). The degree of thermal stability and cooperativity varies in different domains, however NMR and CD argue in each case for the existence of a folded helical core and large unstructured segments. This suggests that the molecular architecture determined from ATS-FL is widespread throughout the *Pf*EMP1 family.

Solution Structure of ATS-25—We used solution NMR restraints including NOE, dihedral angle, global orientation and chemical shifts to determine the structure of ATS-Core (supplemental Table S1). The final structural ensemble includes over 20 restraints per ordered residue, and has a precision of ~0.4 Å and 0.9 Å over all ordered backbone and heavy atoms, respectively. ATS-Core comprises four helices (α1-α4) forming a small globular unit (Fig. 2, *A* and *B*) that packs many conserved aromatic groups (supplemental Fig. S8). Dispersed NMR resonances originating from ordered and buried residues of ATS-Core are unchanged compared with spectra of ATS-25 and ATS-FL (Fig. 1, *B* and *D* and supplemental Fig. S7), indicat-

ing that the structural environment of these residues is identical in all constructs.

Based on this evidence, we calculated a molecular ensemble for ATS-25 starting from the existing ATS-Core structure. The later was modified by including the additional sequence elements in random coil conformation, and the model was minimized using the ATS-Core restraints in addition to chemical shift and hydrogen bonding parameters for the flexible segments. As expected, ATS-25 (Fig. 2*C*) showed no evidence for order along the central flexible element of ATS, the conformation of which is simply restrained into a closed loop by ATS-Core. The degree of compaction in this molecular ensemble was evaluated in terms of the R_g distribution, which centers at ~3 nm (supplemental Fig. S11). A similar measure of compaction was extracted directly from the SAXS data of ATS-25 by using EOM (15), which optimizes an ensemble of chain conformations against the SAXS data using a genetic algorithm. The final optimized ensemble fits the data to a resolution of ~4 Å, and shows a monodispersed R_g distribution also centered on 3 nm (supplemental Fig. S11). This agreement between the NMR-based and SAXS-based ensembles suggests that our NMR model of ATS-25 is representative of the protein compactness in solution.

Solution Studies Do Not Support the ATS-KAHRP Interaction—Past *in vitro* experiments using recombinant ATS and KAHRP demonstrated a binary association for surface-immobilized fragments of these proteins (9–11). The interaction was localized to two regions of each protein, termed K1A and K2A for KAHRP (Fig. 3*A*), and B2 and B3 for ATS (10, 11). The ATS fragments B2 (residues 118–214) and B3 (215–279) correspond broadly to the N-terminal and C-terminal halves of our ATS-25 construct, respectively. B2 and B3 contain only half the helical core of ATS each and, as a result, they are not structured in isolation. Thus, we decided to initially test for the ATS-KAHRP interaction using ATS-25 and KAHRP fragments K1A and K2A.

Surprisingly, when titrating ^{15}N-labeled ATS-25 with unlabeled K1A or K2A we observed no evidence for association in solution (Fig. 3, *B* and *C*). The NMR spectra of ATS-25 show no change in resonance peak position, signal intensity or line width upon titration even under relatively high concentrations of KAHRP fragments. This result prompted us to expand our tests, by using ATS-FL and larger KAHRP fragments (*K1*, *K2*, *K3*, Fig. 3*A*) spanning the entire molecule. Again, however, we did not observe any indication for interactions in the NMR spectra under physiological conditions (supplemental Fig. S12). Because many ATS NMR peaks are overlapped, it was suggested that small resonance perturbations upon KAHRP binding may be masked under the poorly dispersed center of our spectra. Thus, we inverted the labeling pattern in our experiments and tested titrations of ^{15}N K1A and K2A with ATS-FL. As seen in supplemental Fig. S12, the K1A and K2A spectra harbor fewer peaks that are better resolved. However, there were again no significant indications for interaction even when using as much as 500 μM (>20 mg/ml) of ATS-FL.

Given the surprising nature of this result, we decided to test for the ATS-KAHRP interaction using fluorescence anisotropy, which measures molecular tumbling in solution. ATS-FL includes a single cysteine residue, Cys-272, however it is inaccessible as it is buried in the hydrophobic core. Thus, we engi-

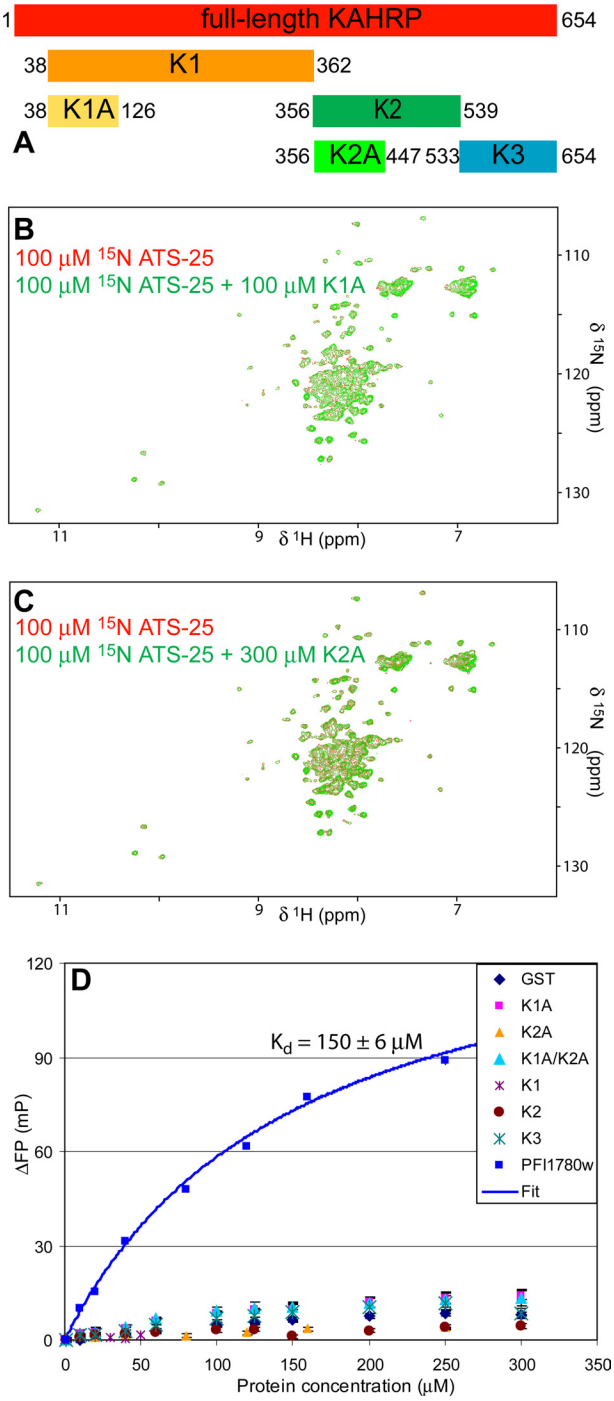

FIGURE 3. **Solution studies of the ATS interactions.** *A*, schematic representation of KAHRP fragments. Shown here is full-length KAHRP from *P. falciparum* 3D7 (*red bar*) as well as the relative sizes and locations of the KAHRP subfragments (K1, K2, K3, K1A, and K2A). The residue boundaries of each construct are indicated. *B*, overlay of NMR spectra of ^{15}N-labeled ATS-25 alone (*red*) or in the presence of unlabeled K1A (*green*). Both spectra were recorded in NMR buffer and 25 °C. *C*, similar overlay of NMR spectra for ATS-25 alone or with K2A. Neither K1A nor K2A produce significant perturbations in the ATS-25 spectra. *D*, fluorescence anisotropy titrations of labeled ATS-FL with KAHRP fragments, GST, or PFI1780w. None of the KAHRP fragments nor GST produced strong anisotropy changes in concentrations up to 300 μM (50 μM for K1 due to limited solubility). PFI1780w titrations yield a binding isotherm that can be fit (*solid line*) to a single site model with a K_d of ~150 μM. Error bars derive from five replicates.

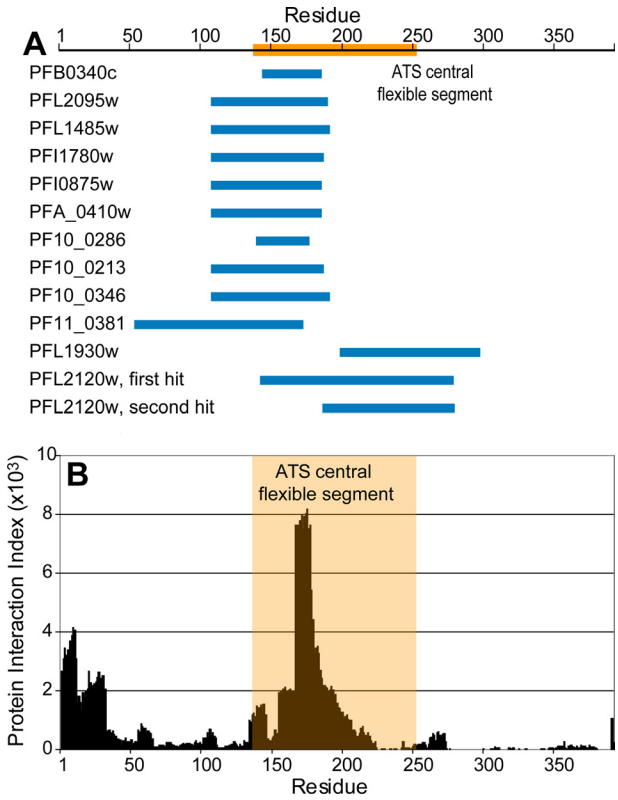

FIGURE 4. **The ATS central flexible segment is a hotspot for protein interactions.** *A*, *top*: schematic representation of the central flexible segment (*orange box*) with respect to ATS-FL. The thirteen *P. falciparum* 3D7 genes found to interact with ATS variants by yeast-two-hybrid methods (21) are noted, and the ATS region of interaction in each case is shown (*blue boxes*). *B*, per-residue protein interaction index for ATS-FL. The central flexible segment is highlighted in *light orange color*.

neered an amino acid substitution, Q150C, located at the central flexible segment of ATS-FL, and specifically labeled the exposed thiol group with fluorescein. Titrations of this ATS-FL variant with KAHRP fragments yielded only small changes in anisotropy (Fig. 3*D*), to a maximum of ~14 mP using 300 μM K1A. In comparison, control experiments with 300 μM glutathione *S*-transferase (GST) yielded an anisotropy change of ~8 mP. Co-incubation of ATS-FL with a 1:1 stoichiometric mixture of K1A and K2A did not alter this result. We conclude that our experiments do not support the existence of a strong ATS-KAHRP interaction in solution. Given the protein concentration used, we cannot exclude the possibility of a very weak interaction, with a affinity constant K_d in the mM range. However, such an interaction would be at least 1,000 times weaker than suggested by previous reports (9–11).

ATS Contains a Conserved Interaction Epitope—Because no interaction between ATS and KAHRP was detected, we attempted to identify alternative binding partners. Analysis of the previously reported Y2H-based *P. falciparum* interactome (21) revealed 13 protein targets that associated with one or more ATS variants. Remarkably, mapping these interactions on the ATS-FL sequence revealed that they all involve parts of the central flexible segment (Fig. 4*A*). Although Y2H methods can lead to false-positive events, we believe that the convergence of multiple interactors on the same ATS target constitutes a strong signal for protein associations.

To provide further evidence for the protein interaction relevance of the central flexible ATS segment, we applied a novel bioinformatics analysis tool that allows for sequence-derived interaction probability assessment, expressed as the protein interaction index (PII). As seen in Fig. 4*B* the ATS-FL sequence yields a single strong PII signal in the central flexible segment of the protein, which suggests a high likelihood for protein-protein interactions in this region. The PII signal is embedded in an ATS-FL epitope spanning residues 161–186 that is highly conserved in the *Pf*EMP1 family (supplemental Fig. S8). Over half the residues in this segment (14 out of 26) are identical in 95% of ATS domains, while 25 out of 26 residues are identical or conservatively substituted in all but one of the 59 *Pf*EMP1 variants in the *P. falciparum* 3D7 isolate. The high level of sequence conservation suggests that this interaction epitope is a generalized feature in the *Pf*EMP1 family.

ATS-FL Interacts with a PHIST Domain—To demonstrate the relevance of the predicted protein interaction epitope in the central flexible segment of ATS, we reviewed the Y2H interactors of Fig. 4 based on their likelihood to be structured, and taking into account the existence of signal peptide sequences that would allow these proteins to be in the same cell compartment as ATS. We choose to investigate PFI1780w since it comprises a PHISTc-type domain, a module class unique to the *Plasmodium* genus (12). A PFI1780w fragment spanning residues 80–280 (henceforth referred to simply as PFI1780w) could be produced recombinantly in *E. coli* and shown to be highly helical and cooperatively folded by CD (supplemental Fig. S4). Titrations of unlabeled PFI1780w with ^{15}N labeled ATS-FL produced substantial changes in the NMR spectra (Fig. 5*A*) as a result of drastic intensity loss for many ATS-FL resonances. This phenomenon is specific, as it was not observed in earlier titrations of KAHRP fragments (supplemental Fig. S12). ATS-FL resonances most affected by PFI1780w include those corresponding to the structured protein core, as well as resonances from residues of the central flexible segment such as Gly-203, Gly-213, and Gly-233 (Fig. 5, *A* and *B*). Unfortunately, the overlapped nature of the two-dimensional ATS-FL spectra prevented us from unambiguously assigning all affected resonances. Titrations of PFI1780w with fluorescein-labeled ATS-FL yield strong changes in anisotropy that can be fit to a K_d of ~150 μM (Fig. 3*D*).

To evaluate whether the ATS central flexible segment is necessary for this interaction we repeated the NMR titrations using ^{15}N-labeled ATS-25 and ATS-Core. As seen in Fig. 5, *B* and *C*, we observed the same disappearance of resonances when using ATS-25 but not ATS-Core. The later construct lacks the central flexible segment and, thus, the protein interaction epitope predicted earlier. We conclude that ATS does interact with other proteins as suggested by the Y2H data, and further that the conserved flexible segment at the ATS center is necessary for association.

DISCUSSION

We present here the first structural data for the intracellular domain of *Pf*EMP1, a crucial link in the malaria cytoadherence system. ATS comprises a largely flexible protein with a small structured core that provides a minimal conformational restraint for a central flexible segment. Substantial unstructured protein segments are common in eukaryotes (22) and are

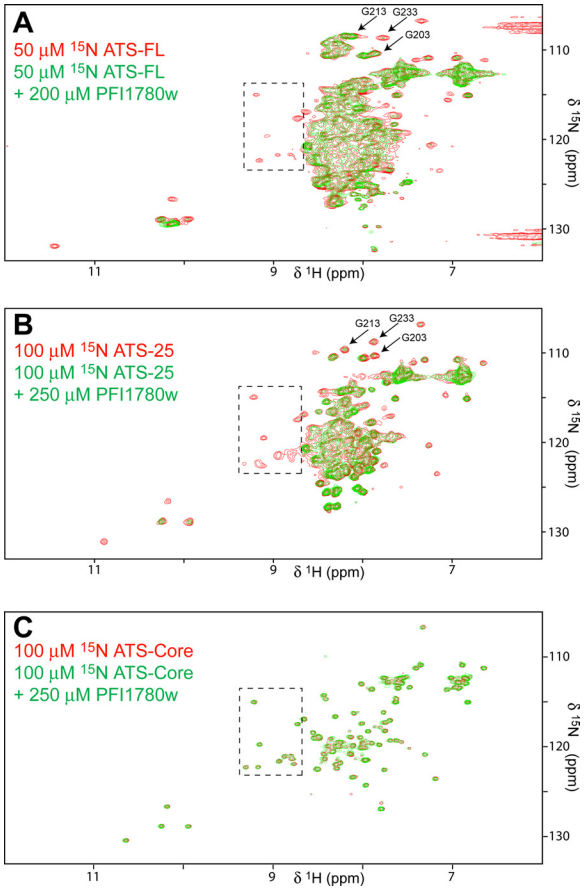

FIGURE 5. **ATS interacts with PFI1780w.** *A*, overlay of NMR spectra of ^{15}N-labeled ATS-FL alone (*red*) or in the presence of unlabeled PFI1780w (*green*). Both spectra were recorded in NMR buffer and 25 °C. *B* and *C*, similar overlay of NMR spectra for ATS-25 (*B*) or ATS-Core (*C*) alone or in the presence of unlabeled PFI1780w. Note the significant loss of signal intensity upon titration observed for many resonances in the ATS-FL and ATS-25 spectra, but not when using ATS-Core. A number of ATS resonances originating from the structured protein core are enclosed in a *dashed box*; resonances originating from specific residues of the central flexible element are labeled.

predicted to exist in as much as 50% of *P. falciparum* proteins (23), a number higher than the average for apicomplexan parasites. The disordered state of these proteins is believed to create large intermolecular interfaces that can provide highly specific but reversible interactions (24). In addition, the conformational flexibility allows for a large volume of space to be searched for interaction partners, a mechanism that has been described as "fly-casting". Nevertheless, flexible proteins constitute a challenge for structural biology since they cannot be crystallized and, instead, need to be described in molecular ensemble terms. It is likely that the flexible nature of ATS is largely responsible for the little information available to date for this system.

How does ATS anchor *Pf*EMP1 to knobs and to host cells? KAHRP is known to be essential for knob formation and efficient cytoadherence based on knock-out experiments (8), thus it is often believed that it interacts directly with ATS (2). Past studies approached this hypothesis using surface immobilized proteins or protein fragments. Under these conditions the affinity of ATS and KAHRP was estimated as 0.2–1.1 μM K_d (10) or even as strong as ~10 nM (9). However, despite the potentially crucial nature of the ATS-KAHRP association no supporting biophysical or *in vivo* data have been presented to date. Despite our efforts, no evidence for this interaction could be seen in solution experiments under physiological conditions, even when using protein amounts more than two orders of magnitude larger than the reported affinity constants. Although this is a negative result, we believe its disclosure is important for the malaria cytoadherence field. Based on our data, the ATS-KAHRP interaction is either strongly dependent on uncharacterized surface phenomena or, alternatively, too weak to be detected in solution, which would imply a K_d in the order of several mM. The physiological relevance of an interaction so weak is, in our opinion, questionable.

What are the alternatives to an ATS-KAHRP interaction? *P. falciparum* exports over 400 proteins to the cytosol of the host erythrocyte (25), thus a selection process was necessary. We turned to the genome-wide Y2H screen performed earlier (21), and identified 13 putative ATS interactors all of which target the central flexible segment of ATS. The same segment was highlighted by a novel bioinformatics method presented here as putative hotspot for protein interactions, and it has markedly high sequence conservation in the *Pf*EMP1 family. It is interesting to note that the single structured element of ATS, its stable helical core, restricts the end-to-end distance of the central flexible segment by forcing it to form a nearly closed loop. This minimal restraint provided by ATS-Core could potentially lower the entropic penalty for protein binding, thus enhancing the interaction affinity.

Our studies show that at least one of the 13 proteins identified by Y2H interacts with ATS-FL in a manner requiring the central flexible segment. PFI1780w comprises a PHIST-type domain, however nothing is known about its function. It is exported to the erythrocyte host (12), while expression profiling (26, 27) and mass spectrometry data (28) show its presence during the parasite blood stage. Therefore, PFI1780w constitutes an interesting novel target for cytoadherence studies related to *Pf*EMP1 function. In addition, the PHIST domain class is specific to the *Plasmodium* genus and it is greatly expanded in *P. falciparum* (12), yet to date no specific function had been assigned to a domain of this type. We hypothesize that PHIST may serve generally as interaction modules linking parts of the parasite intra-erythrocyte protein network.

More generally, we find that the independent convergence of multiple research directions, structural, computational and intermolecular interactions, on the central flexible ATS segment is highly suggestive of its importance in the parasite cytoadherence system. Given the significance of erythrocyte sequestration in disease pathology, we believe this ATS segment may constitute an attractive candidate for studies of targeted intervention.

Acknowledgments—We thank Drs. Amit Sharma and Matthew Higgins for ATS clones, and MR4 for providing us with the P. falciparum 3D7 cDNA library and KAHRP clone. We are grateful to Prof. Iain D. Campbell for support and helpful discussions, Nick Soffe for assistance with the NMR instrumentation, Dr. Steven Johnson for performing the SLS experiment, and Dr. David Staunton for help with mass spectrometry. We acknowledge the ESRF for provision of synchrotron radiation facilities, and Drs. Louiza Zerrad and Silvia Russi for assistance with the BioSAXS beamline.

REFERENCES

1. Haldar, K., and Mohandas, N. (2007) Erythrocyte remodeling by malaria parasites. *Curr. Opin. Hematol.* **14,** 203–209
2. Maier, A. G., Cooke, B. M., Cowman, A. F., and Tilley, L. (2009) Malaria parasite proteins that remodel the host erythrocyte. *Nat. Rev. Microbiol.* **7,** 341–354
3. Kraemer, S. M., and Smith, J. D. (2006) A family affair: var genes, PfEMP1 binding, and malaria disease. *Curr. Opin. Microbiol.* **9,** 374–380
4. Wickham, M. E., Rug, M., Ralph, S. A., Klonis, N., McFadden, G. I., Tilley, L., and Cowman, A. F. (2001) Trafficking and assembly of the cytoadherence complex in *Plasmodium falciparum*-infected human erythrocytes. *EMBO J.* **20,** 5636–5649
5. Roberts, D. J., Craig, A. G., Berendt, A. R., Pinches, R., Nash, G., Marsh, K., and Newbold, C. I. (1992) Rapid switching to multiple antigenic and adhesive phenotypes in malaria. *Nature* **357,** 689–692
6. Chen, Q., Barragan, A., Fernandez, V., Sundström, A., Schlichtherle, M., Sahlén, A., Carlson, J., Datta, S., and Wahlgren, M. (1998) Identification of *Plasmodium falciparum* erythrocyte membrane protein 1 (PfEMP1) as the rosetting ligand of the malaria parasite P. falciparum. *J. Exp. Med.* **187,** 15–23
7. Rasti, N., Wahlgren, M., and Chen, Q. (2004) Molecular aspects of malaria pathogenesis. *FEMS Immunol. Med. Microbiol.* **41,** 9–26
8. Crabb, B. S., Cooke, B. M., Reeder, J. C., Waller, R. F., Caruana, S. R., Davern, K. M., Wickham, M. E., Brown, G. V., Coppel, R. L., and Cowman, A. F. (1997) Targeted gene disruption shows that knobs enable malaria-infected red cells to cytoadhere under physiological shear stress. *Cell* **89,** 287–296
9. Oh, S. S., Voigt, S., Fisher, D., Yi, S. J., LeRoy, P. J., Derick, L. H., Liu, S., and Chishti, A. H. (2000) *Plasmodium falciparum* erythrocyte membrane protein 1 is anchored to the actin-spectrin junction and knob-associated histidine-rich protein in the erythrocyte skeleton. *Mol. Biochem. Parasitol.* **108,** 237–247
10. Waller, K. L., Cooke, B. M., Nunomura, W., Mohandas, N., and Coppel, R. L. (1999) Mapping the binding domains involved in the interaction between the *Plasmodium falciparum* knob-associated histidine-rich protein (KAHRP) and the cytoadherence ligand *P. falciparum* erythrocyte membrane protein 1 (PfEMP1). *J. Biol. Chem.* **274,** 23808–23813
11. Waller, K. L., Nunomura, W., Cooke, B. M., Mohandas, N., and Coppel, R. L. (2002) Mapping the domains of the cytoadherence ligand *Plasmodium falciparum* erythrocyte membrane protein 1 (PfEMP1) that bind to the knob-associated histidine-rich protein (KAHRP). *Mol. Biochem. Parasitol.* **119,** 125–129
12. Sargeant, T. J., Marti, M., Caler, E., Carlton, J. M., Simpson, K., Speed, T. P., and Cowman, A. F. (2006) Lineage-specific expansion of proteins exported to erythrocytes in malaria parasites. *Genome Biol.* **7,** R12
13. Vakonakis, I., Langenhan, T., Prömel, S., Russ, A., and Campbell, I. D. (2008) Solution structure and sugar-binding mechanism of mouse latrophilin-1 RBL: a 7TM receptor-attached lectin-like domain. *Structure* **16,** 944–953
14. Konarev, P. V., Volkov, V. V., Sokolova, A. V., Koch, M. H. J., and Svergun, D. I. (2003) PRIMUS: a Windows PC-based system for small-angle scattering data analysis. *J. Appl. Crystallogr.* **36,** 1277–1282
15. Bernadó, P., Mylonas, E., Petoukhov, M. V., Blackledge, M., and Svergun, D. I. (2007) Structural characterization of flexible proteins using small-angle X-ray scattering. *J. Am. Chem. Soc.* **129,** 5656–5664
16. Konrat, R. (2009) The protein meta-structure: a novel concept for chemical and molecular biology. *Cell Mol. Life Sci.* **66,** 3625–3639
17. Hora, R., Bridges, D. J., Craig, A., and Sharma, A. (2009) Erythrocytic casein kinase II regulates cytoadherence of *Plasmodium falciparum*-infected red blood cells. *J. Biol. Chem.* **284,** 6260–6269
18. Platzer, G., Schedlbauer, A., Chemelli, A., Ozdowy, P., Coudevylle, N., Auer, R., Kontaxis, G., Hartl, M., Miles, A. J., Wallace, B. A., Glatter, O., Bister, K., and Konrat, R. (2011) The metastasis-associated extracellular matrix protein osteopontin forms transient structure in ligand interaction sites. *Biochemistry* **50,** 6113–6124
19. Narang, P., Bhushan, K., Bose, S., and Jayaram, B. (2005) A computational pathway for bracketing native-like structures fo small α-helical globular proteins. *Phys. Chem. Chem. Phys.* **7,** 2364–2375
20. Lavstsen, T., Salanti, A., Jensen, A. T., Arnot, D. E., and Theander, T. G. (2003) Sub-grouping of *Plasmodium falciparum* 3D7 var genes based on sequence analysis of coding and non-coding regions. *Malar. J.* **2,** 27
21. LaCount, D. J., Vignali, M., Chettier, R., Phansalkar, A., Bell, R., Hesselberth, J. R., Schoenfeld, L. W., Ota, I., Sahasrabudhe, S., Kurschner, C., Fields, S., and Hughes, R. E. (2005) A protein interaction network of the malaria parasite *Plasmodium falciparum. Nature* **438,** 103–107
22. Oldfield, C. J., Cheng, Y., Cortese, M. S., Brown, C. J., Uversky, V. N., and Dunker, A. K. (2005) Comparing and combining predictors of mostly disordered proteins. *Biochemistry* **44,** 1989–2000
23. Feng, Z. P., Zhang, X., Han, P., Arora, N., Anders, R. F., and Norton, R. S. (2006) Abundance of intrinsically unstructured proteins in *P. falciparum* and other apicomplexan parasite proteomes. *Mol. Biochem. Parasitol.* **150,** 256–267
24. Dunker, A. K., Cortese, M. S., Romero, P., Iakoucheva, L. M., and Uversky, V. N. (2005) Flexible nets. The roles of intrinsic disorder in protein interaction networks. *Febs J.* **272,** 5129–5148
25. Bonnefoy, S., and Ménard, R. (2008) Deconstructing export of malaria proteins. *Cell* **134,** 20–22
26. Llinás, M., Bozdech, Z., Wong, E. D., Adai, A. T., and DeRisi, J. L. (2006) Comparative whole genome transcriptome analysis of three *Plasmodium falciparum* strains. *Nucleic Acids Res.* **34,** 1166–1173
27. Bozdech, Z., Llinás, M., Pulliam, B. L., Wong, E. D., Zhu, J., and DeRisi, J. L. (2003) The transcriptome of the intraerythrocytic developmental cycle of *Plasmodium falciparum. PLoS Biol.* **1,** E5
28. Bowyer, P. W., Simon, G. M., Cravatt, B. F., and Bogyo, M. (2011) Global profiling of proteolysis during rupture of Plasmodium falciparum from the host erythrocyte. doi: 10.1074/mcp.M110.001636, *Mol. Cell Proteomics* **10,** in press